JOURNAL OF COMPUTATIONAL PHYSICS **145,** 555–574 (1998)
ARTICLE NO. CP986041

Modeling a Limited Region of the Ocean

Amala Mahadevan[1] and David Archer

Department of Geophysical Sciences, University of Chicago, Chicago, Illinois 60637
E-mail: amala@starbuck.uchicago.edu and archer@starbuck.uchicago.edu

Received June 2, 1997; revised June 4, 1998

Many of the difficulties that arise from the specification of open boundary conditions when modeling a limited region of the ocean with the *primitive equations* can be overcome by using a nonhydrostatic set of equations that is well posed in open domains even without the viscous term. We simulate the mesoscale flow in a region of the open ocean using the flow fields from a global circulation model to provide initial and boundary data. Information flow across lateral boundaries is specified using the method of characteristics. By modeling the region at higher resolutions than the fields providing boundary conditions, we are able to resolve more structure and processes in the flow than were detectable from the initial and boundary data. This is of value for studying a region of the ocean in detail at moderate computational cost, if initial and boundary data is available. Shortcomings of the characteristics-based formulation of the boundary conditions and limitations in using such a model to selectively refine a region within a coarser model are also examined.

1. INTRODUCTION

Even though models of the ocean's global circulation are able to deliver higher and higher resolution and accuracy today, there is still a need to model regions of the ocean in greater detail and at lesser cost than is possible with global models. Such regional models must inevitably deal with open boundaries across which there is flow, and their development has been largely impeded by the numerous difficulties associated with open boundary conditions.

The difficulty with using traditional primitive equation models for the three-dimensional flow in a region of the ocean is that the (inviscid) primitive equations (consisting of the horizontal momentum equations, the hydrostatic approximation, and the continuity constraint for an incompressible fluid) are ill-posed in domains with open boundaries [14, 2]. The

[1] Corresponding author. Presently at Department of Applied Ocean Physics and Engineering, Woods Hole Oceanographic Institution, Woods Hole, MA 02543 and Department of Earth Atmospheric and Planetary Sciences, MIT, Cambridge, MA 01239.

0021-9991/98 $25.00

direction of the characteristics at an open boundary can differ for different internal modes of the system. Hence, the number of boundary conditions required at an open boundary cannot be predetermined and local well-posed boundary conditions cannot be designed for this system. Adding sufficiently large viscosity to the primitive equations changes their form and makes them more amenable to open boundary conditions. While eddy viscosity is an acceptable parameterization for subgridscale processes, the well-posedness of the model that describes the physics ought not to be dependent on it. The model's ability to handle open boundaries would then depend on the size of eddy viscosity, and the minimum value required to overcome the ill-posedness may exceed what is representative of subgridscale processes. It is common in such cases to use extra viscosity at the boundaries in the form of sponge layers, or to use special outflow boundary conditions. This is undesirable, as besides stabilizing the solution, viscosity damps out the motions of interest which may be driven by the open boundary conditions within a limited domain.

The momentum equations without the hydrostatic approximation, on the other hand, are well-posed in domains with open boundaries. They cannot, however, always be used in their exact form as a model for large scale oceanographic flow. Such flow is nearly hydrostatic, and the fine balance between the pressure gradient and weight of the fluid (or the fine balance between pressure gradient and the Coriolis term in the case that the hydrostatic balance is subtracted out) in the vertical momentum equation, cannot, in some large-scale situations, be computed to sufficient accuracy. The hydrostatic approximation which assumes the vertical pressure gradient and weight of the fluid to be in exact balance would circumvent this problem by eliminating the vertical momentum equation altogether, but would also render the problem ill-posed when there are open boundaries. Instead, we use an alternate approximation for such situations, that is to allow a greater deviation from the balance between the pressure gradient and weight of fluid than really exists. This results in the so-called *reduced* equations suggested by Browning *et al*. [2]. They are nonhydrostatic in form, and with suitable boundary conditions, are, like the unaltered nonhydrostatic equations, well-posed in domains with open or solid boundaries. The approximation made in these equations ensures a desired relative accuracy in all the solution variables and can in situations, as those treated in this paper, speed up the computation considerably. Since the approximation entails merely a modification to the scaling coefficient in the vertical momentum equation, one can easily revert to the unaltered nonhydrostatic equations when the situation permits.

While the well-posed nonhydrostatic model has the advantage of handling open boundary conditions very smoothly, we must contend with the fact that these equations require computing a three-dimensional pressure field, compared to a two-dimensional one in the hydrostatic case. However, this is not quite as expensive as one would imagine. The hydrostatic nature of large-scale flow renders the equations and, consequently, the Laplacian operator of the pressure in the elliptic pressure equation highly skewed. This inhomogeneity is taken advantage of by using line by line relaxation (or equivalently block relaxation) in greatly speeding up the solution of the three-dimensional elliptic equation for pressure [8]. Thus, the solution procedure is merely two to three times more expensive than the solution of the hydrostatic equations.

In this paper, we demonstrate the use of the nonhydrostatic equations to model large-scale (mesoscale) flow in limited oceanic domains by modeling a $10^\circ \times 10^\circ$ region of the open Atlantic using the flow fields from the global circulation model (GCM) of Semtner and Chervin (1992) [15] (hereafter SC) to provide initial and boundary conditions to the domain. The model has a free-surface, mixed layer and varying bottom topography and produces a realistic picture of the ocean at high resolution (assuming the boundary conditions are

realistic). To test the well-posedness of the model, we exclude the viscous terms from the equations entirely (although they could easily be added if desired) and contrast these results with those from an attempt to use the hydrostatic version of the same model.

While modeling the limited region, we show that we are able to vary the resolution in the domain to observe varying degrees of detail in the flow. Using higher resolution than is used in the GCM enables us to examine the flow in greater detail than was previously possible. The energetics of the finely resolved solution are quite different from the low resolution solution.

Although the nonhydrostatic model overcomes the ill-posedness of the traditional primitive equations in limited domains, limitations arising from the approximation of specifying only normal-to-boundary information through the boundary conditions and from selectively refining a region of the larger domain still exist. To evaluate these shortfalls, we compare the solution in a subregion of the domain with that obtained from modeling the subregion separately by using boundary conditions from the larger domain.

The need for embedded and nested models, in meteorology for weather prediction, as well as in oceanography [12, 20, 17, 4 (and references therein)] to model regional and small-scale phenomena has led to a history of literature on the subject. Some of the best examples of regional primitive equation ocean modeling are due to Spall [16, 18] who succeeds without sponge layers and with what is regarded as a very acceptable value of eddy viscosity. But most would agree, as our results also show, that the use of primitive equation models in open domains is not straightforward, and more often than not requires some special treatment to stabilize the solution.

Our limited area model may be considered "one-way" nested within the SC model, but in this study, we will think of the SC fields merely as boundary and initial data that could alternatively be assimilated from observations. If we were to nest our model within a large-scale model with the purpose of selectively refining regions of the domain, we would need to choose the region of our refinement more carefully, making sure that the resolution of the outer model were sufficient to correctly diagnose the flow on the boundary of the nested refinement.

The ocean model and numerical solution procedure used here is based on that described in [9, 8]. Here, in Section 2, we only briefly present the model equations and solution procedure. In Section 3 we describe the model's implementation in a region of the Atlantic ocean. Section 4 presents our modeling results and observations.

2. A WELL-POSED NONHYDROSTATIC MODEL

2.1. *Model Equations*

We scale the momentum equations for mesoscale flow choosing the advective time scale and assuming that the horizontal pressure gradient is of the order of the Coriolis terms. Using ϵ to denote Rossby number ($=U/FL$, where U is the characteristic velocity, F is the characteristic value of the Coriolis parameter and L is the horizontal length scale), δ to denote the aspect (characteristic depth to length) ratio, and making use of the Boussinesq approximation, we write the dimensionless equations that constitute a nonhydrostatic free-surface model for mesoscale flow as

$$\frac{Ds}{Dt} = \mathcal{S} \tag{2.1a}$$

$$\frac{DT}{Dt} = \mathcal{T} \tag{2.1b}$$

$$\frac{Du}{Dt} + \frac{1}{\epsilon}(gh_x + r_x + \gamma q_x - fv + \epsilon\delta bw) = \frac{\partial \tau_x}{\partial z} \tag{2.1c}$$

$$\frac{Dv}{Dt} + \frac{1}{\epsilon}(gh_y + r_y + \gamma q_y + fu) = \frac{\partial \tau_y}{\partial z} \tag{2.1d}$$

$$\frac{Dw}{Dt} + \alpha\left(q_z - bu + \epsilon\lambda\frac{(u^2+v^2)}{a}\right) = 0 \tag{2.1e}$$

$$u_x + v_y + \epsilon w_z = 0 \tag{2.1f}$$

$$\rho = \rho(s, T) \tag{2.1g}$$

$$\frac{\partial h}{\partial t} + \frac{\epsilon}{\mathcal{F}^2}\left(\frac{\partial}{\partial x}\left(\int_{-d}^{\frac{H}{D}h} u\,dz\right) + \frac{\partial}{\partial y}\left(\int_{-d}^{\frac{H}{D}h} v\,dz\right)\right) = 0, \tag{2.1h}$$

where

$$\frac{D}{Dt} \equiv \frac{\partial}{\partial t} + u\frac{\partial}{\partial x} + v\frac{\partial}{\partial y} + \epsilon w\frac{\partial}{\partial z}.$$

Here x and y are defined as eastward and northward distances along the surface of the globe, z is the distance from the surface of the globe in a direction antiparallel to gravity, and t is time. The Coriolis parameters $f = 2\Omega\sin\phi$ and $b = 2\Omega\cos\phi$ are twice the earth's angular velocity resolved normal and tangential to the earth's surface at a given point whose latitude is ϕ. In the equations they are nondimensionalized by F. The velocity components u, v, w are in the x, y, z directions, respectively. The variable s represents the salinity, T the potential temperature, h the elevation of the free-surface, q the nonhydrostatic component of the pressure, r the hydrostatic pressure due to density variations from the mean, ρ the potential density and a the distance from the center of the earth. All the quantities have been nondimensionalized so that they and their derivatives, too, are order 1. The dimensionless parameter λ is the ratio of the characteristic horizontal length scale to a characteristic value of the earth's radius, and γ is the ratio of the characteristic nonhydrostatic to hydrostatic pressure gradient. $\mathcal{F}$ is the Froude number $(=U/(gD)^{1/2}$, where U and D denote the characteristic velocity and depth of flow) and H/D is the ratio of characteristic free-surface elevation to depth scale. The flux of heat and salt at the ocean surface are modeled by the (nondimensionalized) source terms $\mathcal{T}$ and $\mathcal{S}$. Wind stresses in the x and y direction are denoted by dimensionless τ_x and τ_y. Viscosity and diffusion are neglected in these equations. Equation (2.1g) is an equation of state for the potential density.

The value of the dimensionless coefficient α in (2.1e) is $1/\epsilon^2\delta$. A significant approximation that can be made to these equations [2] is to modify the value of α to be smaller than $1/\epsilon^2\delta$ by a few orders of magnitude. This is helpful in the case of very large scale flow, when numerical limitations prevent us from computing the sum of the parenthesized terms in (2.1e) to sufficient accuracy, and using the original value of α becomes infeasible for computational reasons. One can show from scaling that the error in making this approximation is $O(1/\alpha)$ [9, 2]. A choice of $\alpha = 10^N$ maintains N digits of accuracy in the dimensionless solution variables. Thus, a prodigious choice of α ensures the desired accuracy in the model. Changing the value of α does not modify the form of the equations and both the "exact" nonhydrostatic equations with unaltered α, as well as the so-called

reduced equations with modified α are well-posed in domains with open boundaries at which point-wise boundary conditions can be specified.

In this nonhydrostatic model, it is important that the Coriolis acceleration $(bw, 0, -bu)$ resulting from the tangential component of the earth's angular velocity $\Omega \cos\phi$ not be neglected. The reason for this is made clearer when the hydrostatic balance is subtracted out of the equations as is done in this formulation. The total fluid pressure is written as the sum of a hydrostatic component p^h and a nonhydrostatic component q. Here p^h is defined such that

$$\frac{\partial p^h}{\partial z} + \rho g = 0, \tag{2.3}$$

where g denotes the acceleration due to gravity. Using (2.3), the scaled vertical momentum equation reduces to

$$\frac{Dw}{Dt} + \frac{\gamma}{\epsilon^2\delta^2} q_z - \frac{1}{\epsilon^2\delta} bu + \frac{\lambda}{\epsilon\delta} \frac{(u^2 + v^2)}{a} = 0. \tag{2.4}$$

The last term in this equation is due to the curvature of the earth. The largest term in the vertical momentum equation is the Coriolis acceleration which ought not to be neglected. It is balanced by q_z which must be the same order in magnitude. This implies that

$$\gamma = \delta \tag{2.5}$$

or that the ratio of the characteristic nonhydrostatic to hydrostatic pressure gradient is of the order of the aspect ratio.

From (2.3), we see that the horizontal pressure gradient in the x (and similarly y) direction is then given by

$$\rho_0^{-1} p_x = \rho_0^{-1}\left(p_x^h + q_x\right) = g h_x + g \frac{\partial}{\partial x} \int_z^h \frac{(\rho - \rho_0)}{\rho_0}\, dz + \rho_0^{-1} q_x, \tag{2.6}$$

where ρ_0 is the mean potential density, h is the free-surface elevation, and z is the depth at which the pressure gradient is derived. In the equations above we use r to denote the baroclinic component of the pressure $g\int_z^h (\rho - \rho_0)/\rho_0\, dz$.

Formulating the model with a free-surface avoids the use of the rigid lid boundary condition $w = 0$ at the free-surface and has some other advantages: (a) It enables us to easily decompose the pressure into hydrostatic and nonhydrostatic components and, thus, subtract the hydrostatic balance out of the vertical momentum equation. When using a modified value of α ($\ll 1/\epsilon^2\delta$), this ensures that the three central bands of the matrix arising from the discretizaton of the elliptic pressure equation are much greater than the off-center ones, thus enabling considerable speedup in the solution procedure. (b) We can use a Dirichlet boundary condition when solving for the nonhydrostatic pressure field (although there are other methods to remove the nonuniqueness and the Neumann problem poses no difficulty [G. L. Browning, personal communication]). (c) Free-surface elevation is of interest in oceanography, particularly with the advent of satellite altimetry.

2.2. *Boundary Conditions*

It is shown by Majda [10] that the boundary conditions for the incompressible Euler equations are the same as those for the compressible case. The boundary conditions for

(2.1) can be derived by examining the characteristics (in a direction perpendicular to the boundary) of the equivalent compressible system of equations that retains the time dependent pressure equation,

$$\frac{Dp}{Dt} + \frac{\epsilon}{\mathcal{M}^2}(u_x + v_y + \epsilon w_z) = 0, \tag{2.7}$$

in place of the incompressibility condition (2.1f). Boundary conditions are to be prescribed along incoming characteristics. The characteristic equations in the x directions (written out in [9, Section 4c]) indicate that the following boundary conditions can be specified at a boundary normal to the x direction for a well-posed problem. At *solid boundaries*, the normal velocity u is zero. This is adequate information as there is only one incoming characteristic. At *inflow boundaries* (boundaries where fluid enters the domain), five of the six characteristics are incoming and we need to specify five out of the six variables u, v, w, s, T, p. Alternatively, we could specify v, w, s, T and a combination of u and p that is of the form $u + p/\sqrt{\alpha\epsilon}$. We choose to specify u, v, w, s, T to describe the velocity and density of the incoming fluid. At *outflow boundaries* (boundaries where fluid exits the domain), one characteristic is incoming and we need to specify either the normal velocity or the pressure (or a combination of the two which is of the form $u - p/\sqrt{\alpha\epsilon}$). Likewise, boundary conditions can be written for any boundary by examining the characteristics in the direction normal to it.

At the *free-surface* the pressure is zero. Hence, the nonhydrostatic component of the pressure $q = 0$. It is necessary to specify either the total flux in and out of the domain or the height of the free-surface at the lateral boundaries in order to compute the free-surface elevation in the domain.

2.3. *Numerical Solution*

We use a finite volume method for the numerical solution of the equations. The procedure, described in detail in [8], uses a three-stage Runge Kutta scheme to integrate the equations in time. Within each of the three-Runge Kutta stages, we compute the advection terms using the second-order quadratic upstream interpolation scheme "QUICK" [6], compute the free-surface elevation by solving a two-dimensional elliptic equation, solve for the "hydrostatic" horizontal velocities, compute the nonhydrostatic pressure field q by solving a three-dimensional elliptic equation using the multigrid technique, and finally compute the divergence-free velocity.

Treatment of the Coriolis terms. We find, that for the sake of stability, it is better to lump $(1-\gamma)$ times the Coriolis terms $fu, -fv$ with the hydrostatic pressure gradient and γ times $fu, -fv$ with the nonhydrostatic pressure gradient. We essentially model the Coriolis terms explicitly; i.e., we use previously computed velocities for the Coriolis terms. The disadvantage of this is that the numerical solution admits inertial oscillations. These are triggered by disturbances at the open boundaries and may need to be filtered from the vertical velocity field if it is to be used.

2.4. *Choice of α*

Computations performed by Newberger and Allen [13] with the reduced (using modified α) and exact (using the original α) nonhydrostatic equations suggest that it is best to modify

α as sparingly as possible. However, these computations, as well as those of Marshall *et al*. [11] that compare the hydrostatic and exact nonhydrostatic equations, are in a relatively small domain of 100–200 km horizontal extent and use a relatively very high resolution ($\sim$1 km).

At the larger scales and coarser resolution that we are dealing with, we find that there are substantial advantages in modifying α. Besides overcoming the numerical accuracy problem on account of the large value of α that we are contending with, we find that a certain amount of modification to α speeds up the solution process considerably. Performing some test calculations in an ocean basin with $\alpha = 100, 1000, 10000$ for a flow where the true value of α, $1/\epsilon^2\delta = 10000$, and the resolution is 0.4° (as in the example here), we find that the solutions with $\alpha = 1000$ and $\alpha = 10000$ are indistinguishable, while the solution with $\alpha = 100$ shows some differences. Further, the solution process with $\alpha = 1000$ is 6.5 times faster than that when $\alpha = 10000$. Being satisfied with its accuracy, we use $\alpha = 1000$ for the 0.4° and 0.2° resolution runs, and $\alpha = 4000$ for the 0.1° resolution run performed here. Scaling analysis [9, 2] shows that the relative error in the approximate equations that use a modified α scales as α^{-1} for values of α less than its original value $1/\epsilon^2\delta$.

3. MODEL APPLICATION TO A REGION OF THE OPEN OCEAN

3.1. *Domain and Forcing*

We have chosen a region 30°–$40^\circ N$ and 60°–$50^\circ W$, east of Bermuda in the Atlantic ocean, as a testbed for the model with open lateral boundaries on all sides. The region is a convergence zone for surface currents and is characterized by eddies and fronts. The model is run for a period of 4 months, initializing it with the Semtner–Chervin (SC) flow fields of July 28, 1987. The choice of region and time of year for the model runs was motivated by wanting to study the vertical transport of phytoplankton supporting nutrients into the euphotic layer of the ocean by eddies and fronts [7]. The year itself is chosen ad hoc.

We characterize the mesoscale flow in this region by choosing the horizontal length scale $L = 100$ km, vertical scale $\mathrm{D} = 1000$ m, horizontal velocity $U = 1$ m/s and characteristic Coriolis parameter $F = 10^{-4}$/s. Thus the Rossby number $\epsilon = 0.1$, aspect ratio $\delta = 10^{-2}$, and ratio of nonhydrostatic to hydrostatic pressure $\gamma = 10^{-2}$. The characteristic vertical velocity $W = \epsilon\delta U = 10^{-3}U$.

The model domain is defined by four vertical lateral faces, the ocean surface, and the sea bed. The domain is initialized and driven at the lateral boundaries with flow fields from the 0.4° resolution[2] Semtner–Chervin (SC) model. These flow fields are available at 3-day intervals on a 0.4° resolution latitude–longitude grid which is stair-stepped to fit the topography with variable grid spacing in the vertical. They are interpolated in time and space onto our model grid (described in the next section). We run the model at horizontal resolutions of 0.4°, 0.2°, and 0.1° with a time step of 50 min to satisfy the CFL condition. The model may be considered as nested or embedded within the SC model in a noninteractive or passive manner.

[2] This is better known as the (1/4)-degree model in the literature. It uses a Mercator grid, the spacing of which is approximately 0.4° in the region modeled by us, but globally averages to about 0.25°.

Topographic data is extracted over a large region of the Atlantic containing the model domain on a $5'$ grid and is smoothed with several passes of a Laplacian filter so that it may be smoothly represented at 0.4° resolution. The topography from the $5'$ grid is then interpolated onto the 0.4°, 0.2°, and 0.1° grids used in the simulations. The smoothing is done prior to the interpolation so that the bathymetry is consistent between the low and high resolution runs. As in the SC model, we relax salinity and temperature in the surface layer to Levitus monthly climatological sea surface temperature and salinity with an e-folding time of one month. We also apply the Hellerman and Rosenstein [5] monthly climatological windstress at the surface (SC used the European Centre for Medium-Range Weather Forecasts' (ECMWF) winds for the specific period). The wind has a negligible effect on the dynamics at the small time and spatial scales of interest, but plays a role in determining the mixed layer depth. We impose forcings of heat, salt and wind, similar to SC, in order to maintain compatibility with the SC flow which we use as initial and boundary conditions. The monthly climatological forcing imposes the seasonal variation that is observed in the ocean. While the higher resolution runs can be forced at finer scales and can handle more topographic detail, we use a consistent forcing for all the different resolutions. This is to isolate the effect of the grid resolution from the effect of finer scale forcing on the solution. In reality, one may of course wish to take advantage of prescribing the forcing and geometry at higher resolution when possible.

3.2. *Grid*

Viewed from above, the domain is discretized along lines of latitude of longitude as in the SC model. We use three different horizontal resolutions for our numerical simulations: 0.4° (actually $0.4^\circ \times 0.33^\circ$ as in the SC model), 0.2°, and 0.1°. The 0.4° grid uses 24×28 grid cells to discretize a region that is approximately $10^\circ \times 10^\circ$; the 0.2° and 0.1° grids use 48×56 and 96×112 grid cells, respectively.

In the vertical, our grid is not coincident with the vertical boxes of the SC model, but it is a smoothly boundary-fitted "sigma" grid comprised of four regions as shown in Fig. 1. The topmost layer of grid cells is the *mixed layer*, whose depth varies as the free-surface elevation and mixed layer depth change. The mixed layer depth is modeled using the bulk mixed layer model of Chen and Rothstein [3]. It varies between 10 and 125 m in response to the wind, temperature, and salinity forcing. Below the mixed layer is a finely discretized thermocline region, consisting of eight layers and extending to 510 m depth in this simulation. The mid-region, extending from 510 m to 2510 m and consisting of 10 layers in this case, has horizontal grid surfaces, and the abyssal region consisting of five layers has a "sigma" grid that follows the topography. In each section, the grid is exponentially stretched so as to achieve a grid whose spacing increases smoothly with depth. We use a total of 24 layers in the vertical, compared to a maximum of 20 boxes in the SC model. By restricting the topography-fitted "sigma" grid to the bottommost section consisting of five layers in this case, most of the grid surfaces are maintained horizontal or nearly horizontal, especially in the stratified region of the water column. It is advantageous that the grid layers are nearly parallel to the stratification when computing the horizontal hydrostatic pressure gradients in the sigma coordinate system.

The vertical grid is consistent for all the different horizontal resolutions used here. Comparative runs with increased vertical resolution revealed that the flow is more sensitive to increasing the horizontal resolution rather than the vertical resolution. Hence we concentrated on refining only the horizontal grid in this study.

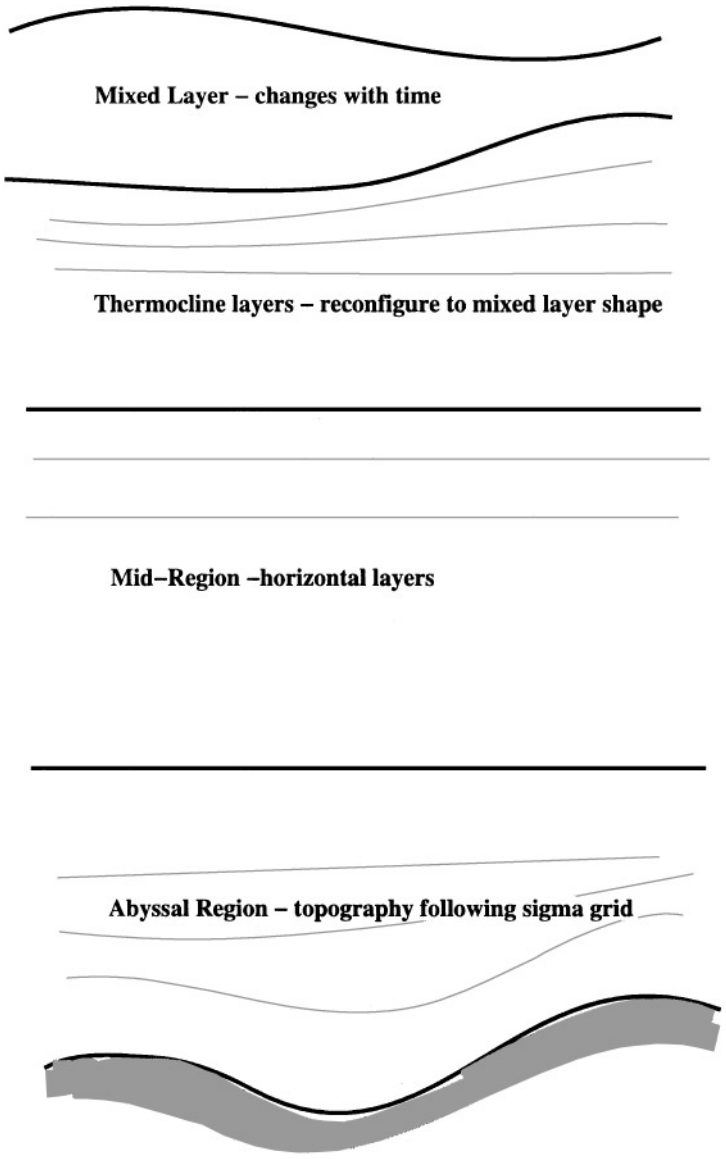

FIG. 1. A schematic vertical section of the grid showing its four sections: the mixed layer, the thermocline region, the mid-region comprising horizontal layers and the abyssal region consisting of the topography-following sigma grid. In each region we use a smooth exponential stretching to achieve an increasing grid spacing with depth within each region as well as overall.

Discretization of pressure gradients on a "sigma" grid. A notorious problem with a topographically fitted sigma grid is that large errors can occur in computing the horizontal gradient of the pressure, when the sigma surfaces are steeply tilted. This is because the horizontal pressure gradient is the sum of the pressure gradient along the sigma surface and the pressure gradient in the vertical, each multiplied by a coefficient of grid curvature. Since the stratification in the fluid is almost horizontal, the terms must nearly cancel out. But cancellation errors can give rise to erroneous pressure gradients that accelerate the flow. To minimize this sort of error, we take two precautions. First, we restrict the topographic

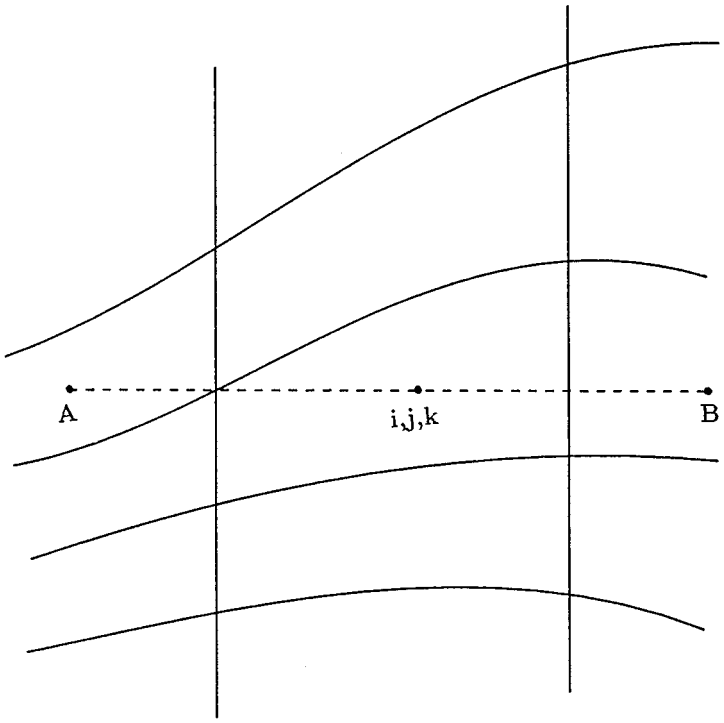

FIG. 2. The horizontal gradient of the hydrostatic pressure due to density variations is evaluated by taking differences in the pressure at the horizontal level at which the gradient is to be evaluated. Thus, the horizontal pressure gradient at cell *i,j,k* is evaluated by taking the difference of the hydrostatic pressure evaluated at points such as A, B (and two others outside the plane of the paper) along the horizontal plane denoted by the dotted line. This alleviates the error that may occur from inaccuracy in computing the cancellation between terms when the pressure gradient is evaluated in the sigma grid system.

sigma grid to the bottom five layers which are nearly homogeneous in most parts. The rest of the grid surfaces are horizontal or nearly horizontal. Second, we compute the horizontal pressure gradients by taking differences only along horizontal surfaces. To do this we compute the pressure due to the fluid weight in adjoining cells at the horizontal level of the cell where the pressure gradient is being evaluated (see Fig. 2). This involves computing the pressure in adjoining grid cells at a point that may lie above or below the cell center.

3.3. *Initialization and Boundary Implementation*

We linearly interpolate the SC model data on to our model grid at the boundaries and throughout the domain at initialization. Since the available SC model flow fields are at 3-day intervals, we also use linear interpolation between the 3-day separated fields to provide boundary data at intermediate times. The interpolation at boundaries is not mass conserving, but other authors [17] using nested models have experienced trouble with conservative interpolation schemes and found strict mass conservation to not be necessary.

We use the interpolated SC data to determine whether a grid cell face on a lateral boundary is an inflow or outflow face, or whether fluid is entering or leaving the grid cell at that face. If it is an inflow face, we specify the three velocity components, salinity, and temperature at the grid cell-center. We also specify the influx on the cell face. If it is an outflow face,

we specify merely the velocity component normal to the face, and the resulting outflux on the cell face. The sum of influx and outflux over the boundary column of cells provides the boundary condition for the elliptic equation for free-surface elevation. We chose to use this rather than the free-surface elevation itself at the boundary.

Pressure as an alternative outflow BC. In the simulations presented here, we specified the normal outflow velocity as an outflow boundary condition. An alternative would be to specify the pressure at the outflow. Since the nonhydrostatic component of the pressure is not available from the hydrostatic SC model data, we tried specifying a pressure derived by integrating the vertical momentum equation with $Dw/Dt = 0$ at the outflow. Since the vertical nonhydrostatic pressure gradient q_z is in near balance with the Coriolis acceleration bu in the vertical momentum equation (2.1e), the value of q is primarily set by this balance, and there is no significant difference in the solution using either of the two boundary conditions at the outflow. We found it simpler to specify the outflow velocity and continued to use this as the boundary condition at outflow.

Conserving the total fluid volume over time. In order to keep the mean sea surface from dropping or rising with time, we impose the constraint that at a given instant, the flow out of the domain equals the flow into the domain. We modify the interpolated outflow velocity values by the minimum possible to meet this constraint. This results in all the outflow fluxes being modified by a small constant at each time step. The adjustment would not be necessary if the interpolation from the SC grid to our grid were mass conserving, or if we could obtain more accurate boundary conditions that did not result in a significant mass flux and unrealistic sea level change with time.

Region in which nonhydrostatic pressure develops. The nonhydrostatic pressure field is not specified at the boundary. Thus there is a small region near the boundary in which the flow field adjusts from being hydrostatic outside the domain, to being nonhydrostatic inside the domain. We allow a two grid-cell-wide region outside of the lateral boundaries for setting up the nonhydrostatic pressure field. The horizontal velocity boundary conditions are prescribed outside of this two cell-wide region to allow the nonhydrostatic pressure field to develop before getting to the domain boundary, where s, T, and w are specified. The vertical velocity within this region is unreliable because the nonhydrostatic pressure is not fully developed, and we avoid using it to compute the advection of variables.

3.4. *The Hydrostatic Counterpart*

The nonhydrostatic model may be converted in to a hydrostatic one by setting the dimensionless coefficient γ in (2.1c) and (2.1d) to 0. The horizontal momentum equations then reduce to the hydrostatic horizontal momentum equations. Since the flow is incompressible, the vertical velocity computed will inevitably be the hydrostatic one, even if we compute it from the pressure q as in the nonhydrostatic case. To compare the hydrostatic and nonhydrostatic calculations in a consistent way, we maintain the same solution method for them both and change only the nonhydrostatic parameter γ. In the nonhydrostatic model, $\gamma = \delta$, the aspect ratio. In the hydrostatic model, $\gamma = 0$.

3.5. *An Embedded Subregion*

As a way to evaluate the performance of the boundary conditions, we model the interior $5^\circ \times 5^\circ$ subregion of the $10^\circ \times 10^\circ$ region using boundary conditions from the outer region.

We then compare the solution obtained in the subregion when it is modeled separately with that obtained from modeling the entire $10^\circ \times 10^\circ$ region. If the boundary conditions were perfect, the solution obtained in the subregion by the two methods would be identical. However, the boundary conditions are only prescribed along characteristics normal to the boundary and have their limitations. The objective of this comparison, which we perform with the 0.2° resolution model, is to evaluate how well the boundary conditions can simulate the desired flow in the subregion.

A further question concerns the use of such limited area models to selectively refine a small region of a larger coarse grid calculation. If fine scale structure is developed near the boundaries of the finely resolved region, then there is the concern that the underlying coarse grid that is incapable of resolving this fine structure will not provide the right boundary conditions to the fine grid. To investigate this, we use 0.1° resolution on the $5^\circ \times 5^\circ$ subregion of the domain modeled at 0.2° resolution. The solution in the subregion is then compared to the 0.2° resolution solution and also to the case when the entire domain is modeled at 0.1° resolution.

4. RESULTS AND DISCUSSION

We are able to use the nonhydrostatic model with open lateral boundaries on all sides, even when the equations contain no viscous terms. We use different resolutions (0.4°, 0.2°, and 0.1°) to model a region of the ocean for a period of 4 months, using the 0.4° resolution SC flow to prescribe initial and boundary conditions.

When we attempt to run the hydrostatic version of the same model at the coarsest resolution (0.4°), we find that disturbances propagate inward from the open boundaries, growing rapidly with time. The model fails catastrophically within the first day and a half of model simulation. (See Fig. 3a.) On the other hand, we have no trouble running both hydrostatic and nonhydrostatic versions of the same model for long periods of time in an enclosed domain (a channel with solid boundaries and periodic inflow–outflow on the east–west walls, a snapshot of which is shown in Fig. 3b). We infer therefore that the failure of the hydrostatic model in the open ocean is a consequence of its ill-posedness in open domains. We would need to make some modification, such as introducing eddy viscosity or some special

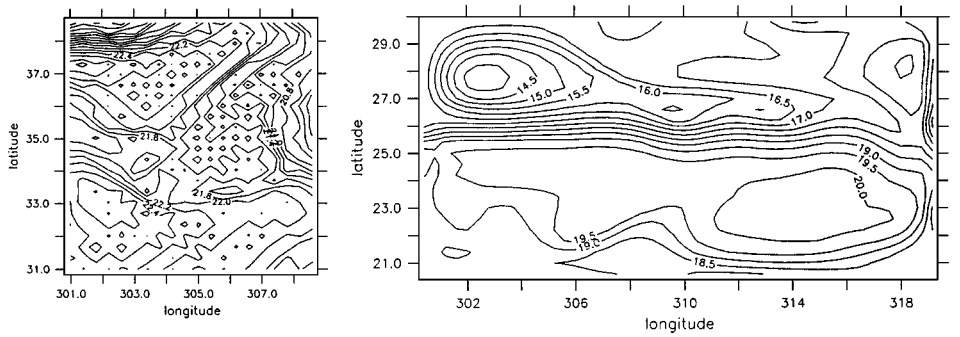

FIG. 3. The temperature field one grid-point below the surface in the hydrostatic model (a) with open boundaries on all sides just 40 time steps (of 50 min) after initialization and (b) in an enclosed channel with an east–west throughflow 1 year after initialization. Boundary conditions in the enclosed channel allow no flow through the solid walls and are periodic in the east–west direction through the inflow and outflow section.

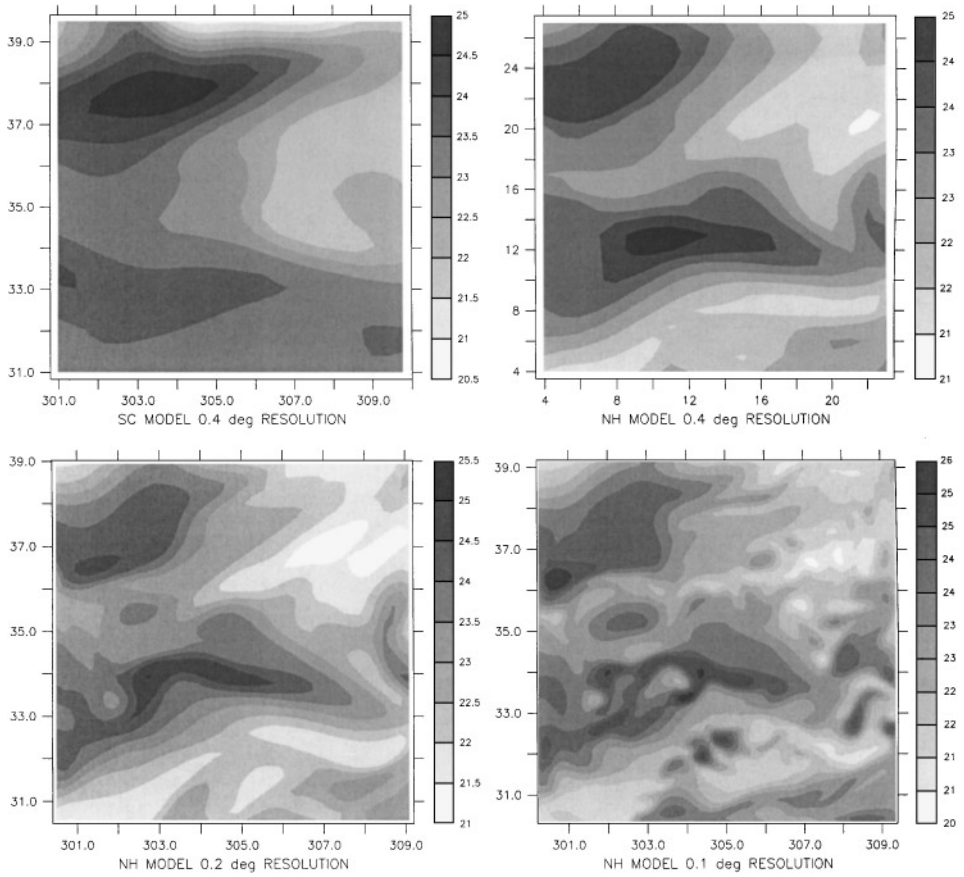

FIG. 4. The temperature field on day 60 of the simulation approximately 44 m below the sea surface (one grid-point below the topmost in our model). The first panel shows the temperature from the 0.4° resolution SC model at the same time, but interpolated in the vertical onto our model grid. The second (top right), third (lower left), and fourth (lower right) panels show the temperature predicted by our model when using a horizontal grid resolution of 0.4°, 0.2°, and 0.1°, respectively. The vertical grid in all our model runs is the same. The initial and boundary conditions for all model runs were interpolated from the SC flow fields shown in the first panel.

boundary treatment that is not necessary in the nonhydrostatic model to stabilize the hydrostatic solution.

Modeling a region of interest at higher resolution than the fields providing boundary conditions is of value if resolving processes that were omitted at coarser resolution. Figure 4 shows the temperature field from the SC model and from our 0.4°, 0.2°, and 0.1° model embedded within a $10^\circ \times 10^\circ$ region of the Atlantic, 60 days after initialization. Increasing resolution has the effect of resolving a lot more of the eddy and frontal structure than was captured in the 0.4° resolution model. The higher resolution model runs exhibit a greater length of frontal zone across which properties change rapidly. Since much of the vertical motion in the ocean occurs at fronts [19, 1], resolving the frontal structure and eddies has considerable implications in modeling the vertical exchange of properties between the surface and deep ocean. Increased resolution enhances, for example, the vertical transport of nutrients for phytoplankton production [7], heat and salt fluxes, and the exchange of oxygen, carbon dioxide, and other atmospheric gases. The difference between the 0.1° and coarser resolution results is particularly striking as the internal Rossby radius of deformation,

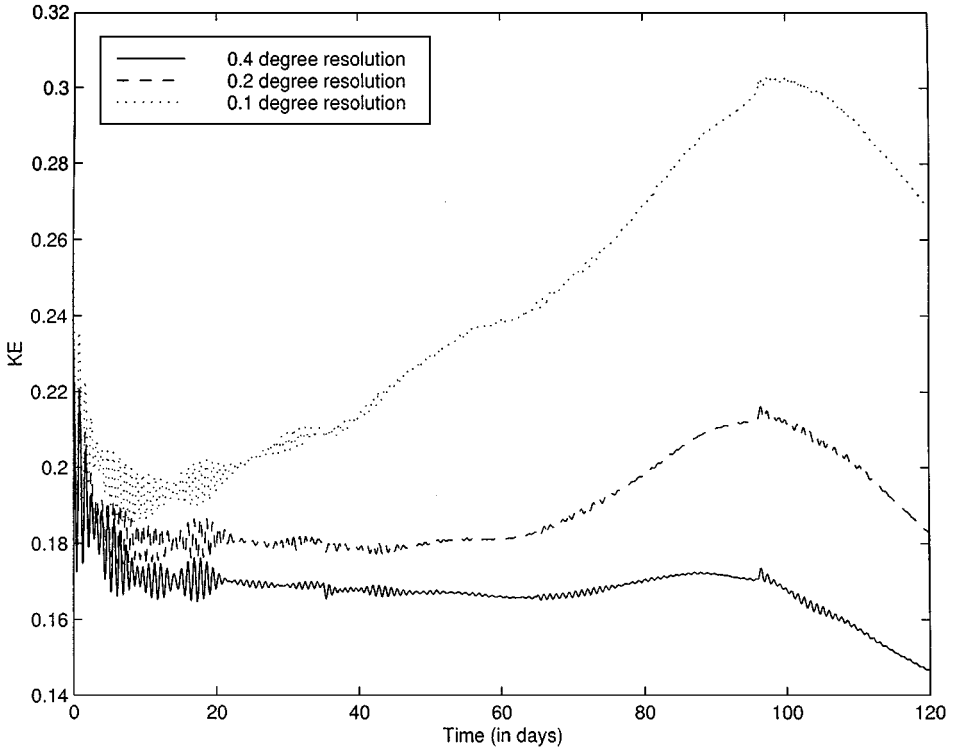

FIG. 5. The kinetic energy (KE) integrated over the volume of the domain and normalized, plotted as a function of time for the different resolution model runs. $\mathrm{KE} = \int_\Omega (u^2 + v^2 + w^2)\, d\Omega$, where Ω denotes the volume of the domain, and is computed as $\Sigma(u_i^2 + v_i^2 + w_i^2)\Delta\Omega_i$, where i denotes the grid cell.

which is the natural length scale of eddies formed by baroclinic instability in the ocean, gets resolved on the 0.1° grid.

The finely resolved flow is more energetic than the coarsely resolved one, by a factor of 1.2–1.8 (see Fig. 5). The kinetic energy builds up over a period as more small-scale structure develops in the flow field at higher resolutions. The energy residing at various length scales of the flow also differs between the different simulations. The coarser resolution runs are unable to resolve the scale at which most of the energy resides in the fine scale calculation. In Fig. 6 we plot the power spectral density of the horizontal velocity components in the layer below the mixed layer averaged along x and y directions on day 60 of the model run. The 0.1°, 0.2°, and 0.4° models exhibit their highest peaks at wavelengths of approximately 0.5°, 1.2°, and 2.4°, respectively. The 0.2° and 0.4° models are unable to represent the peak at 0.5° wavelength, and the 0.4° model is unable to represent the peak at 0.5° and 1.2° wavelength. The coarser resolution runs seem to exaggerate the energy content in the larger wavelengths while being unable to represent the smaller wavelengths.

With increasing resolution, the model becomes more sensitive to the numerical method and interpolation and is more difficult to run for longer periods of time. This is because

FIG. 6. The power spectral density of the horizontal velocity components in the layer below the mixed layer on day 60 of the model run for the different resolutions. In (a) the u velocity is averaged in the E–W direction and in (b) the v velocity is averaged in the N–S direction.

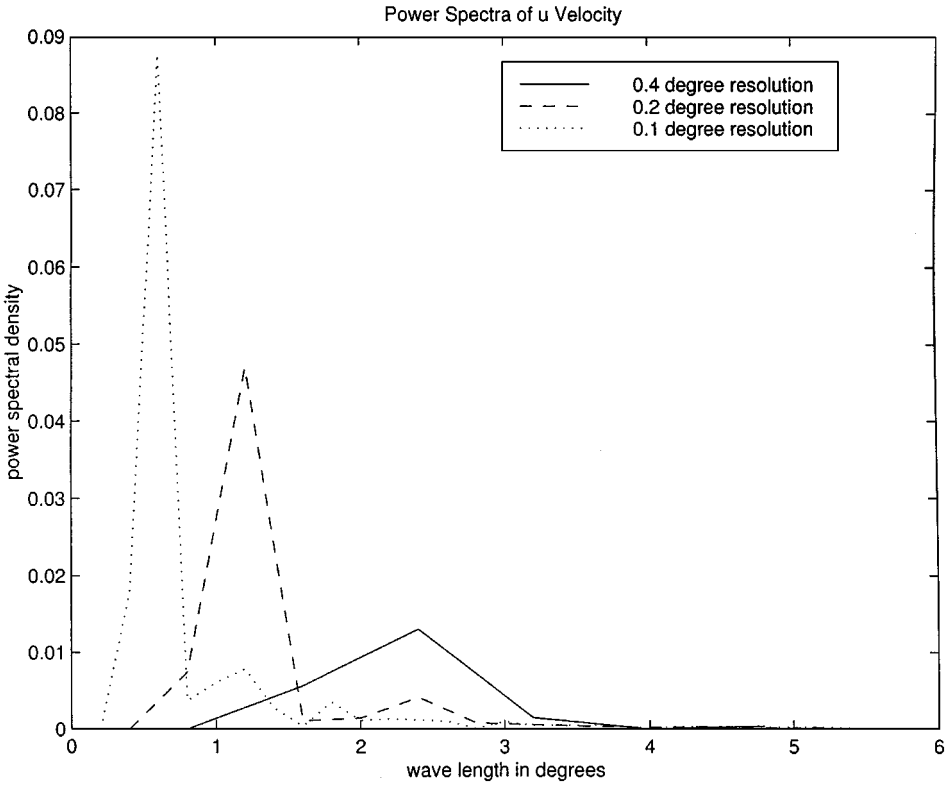
Power Spectra of u Velocity
0.4 degree resolution
0.2 degree resolution
0.1 degree resolution
power spectral density
wave length in degrees
0.09
0.08
0.07
0.06
0.05
0.04
0.03
0.02
0.01
0
0
1
2
3
4
5
6

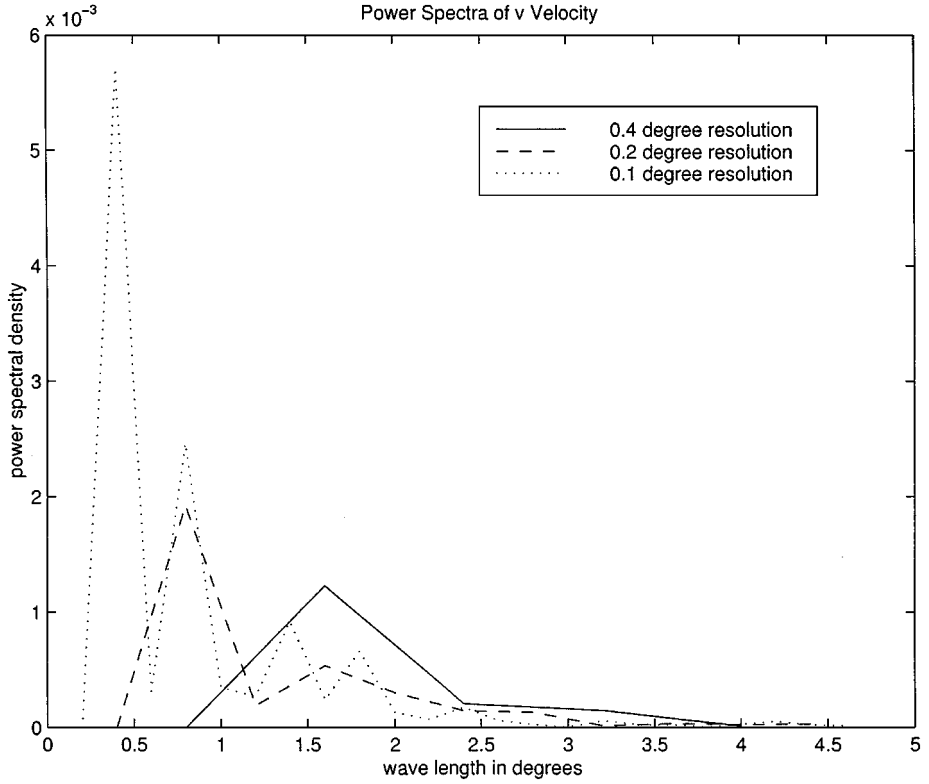
Power Spectra of v Velocity
x 10^-3
0.4 degree resolution
0.2 degree resolution
0.1 degree resolution
power spectral density
wave length in degrees
6
5
4
3
2
1
0
0
0.5
1
1.5
2
2.5
3
3.5
4
4.5
5

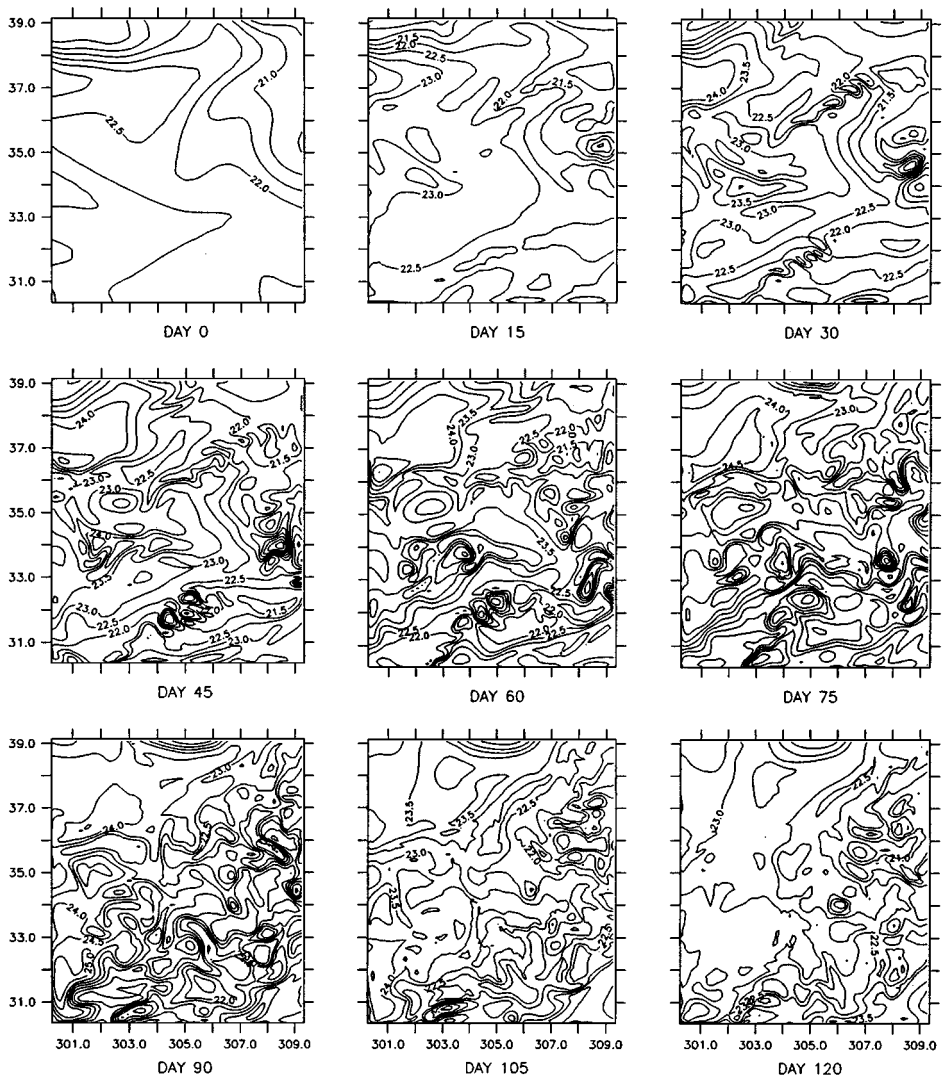

FIG. 7. Time evolution (progressing from left to right, top to bottom) of the temperature field in the 0.1° resolution model. Each snapshot is separated by 15 days, starting with the initial field on July 28, 1987 and progressing through 120 days. The figures display the fields one grid layer below the surface mixed layer. The flow field is initially smooth because we have initialized the model by interpolating data from the 0.4° resolution SC model. The change in mean temperature over time is largely due to the surface heat flux prescribed in the model.

FIG. 8. The temperature (upper four plots) and velocity fields (lower four plots) on day 60 of the simulation approximately 240 m below the sea surface (5 grid points below the topmost in our model) plotted within the interior $5^\circ \times 5^\circ$ subregion of the $10^\circ \times 10^\circ$ domain. In each set of four plots, the first plot (upper left) shows the subregion modeled at 0.2° resolution with boundary conditions from the 0.2° resolution simulation of the $10^\circ \times 10^\circ$ domain, the same subregion of which is plotted below (lower left). The upper right shows the subregion modeled at 0.1° resolution, using the same 0.2° boundary conditions. It is compared to the subregion extracted from the 0.1° resolution model simulation of the entire domain (lower right).

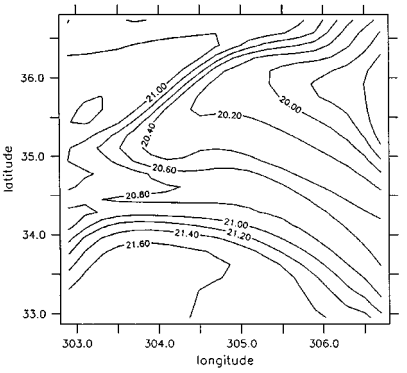
latitude
longitude
36.0
35.0
34.0
33.0
303.0
304.0
305.0
306.0
21.00
20.40
20.20
20.00
20.60
20.80
21.40
21.20
21.60

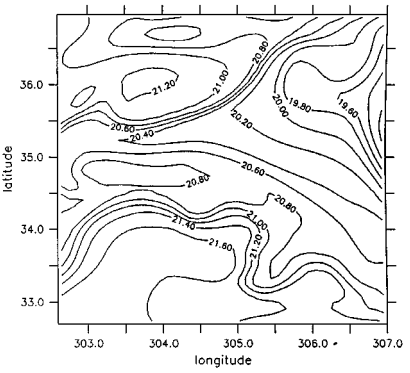
latitude
longitude
36.0
35.0
34.0
33.0
303.0
304.0
305.0
306.0
307.0
21.20
21.00
20.80
20.60
20.40
20.20
20.00
19.80
19.60
21.40
21.60

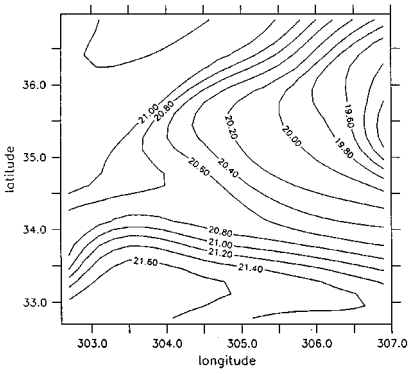
latitude
longitude
36.0
35.0
34.0
33.0
303.0
304.0
305.0
306.0
307.0
21.00
20.80
20.20
20.00
19.80
20.60
20.40
21.60
21.40
21.20

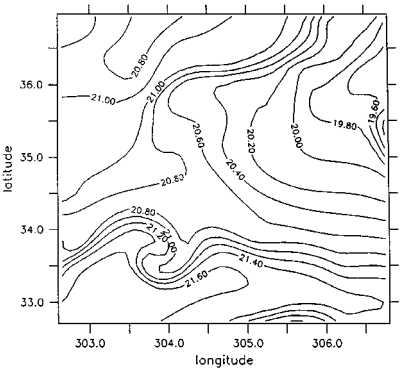
latitude
longitude
36.0
35.0
34.0
33.0
303.0
304.0
305.0
306.0
21.00
20.80
20.60
20.40
20.20
20.00
19.80
19.60
21.40
21.60

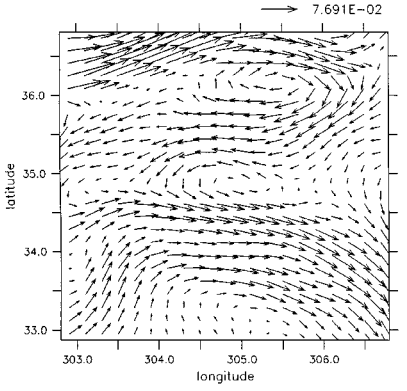
7.691E-02
latitude
longitude
36.0
35.0
34.0
33.0
303.0
304.0
305.0
306.0

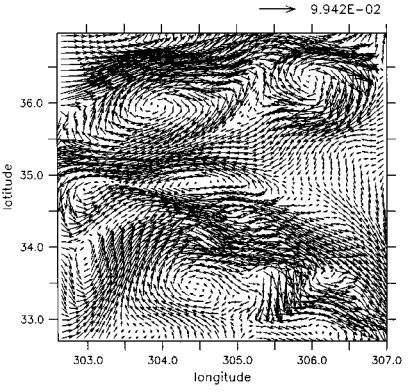
9.942E-02
latitude
longitude
36.0
35.0
34.0
33.0
303.0
304.0
305.0
306.0
307.0

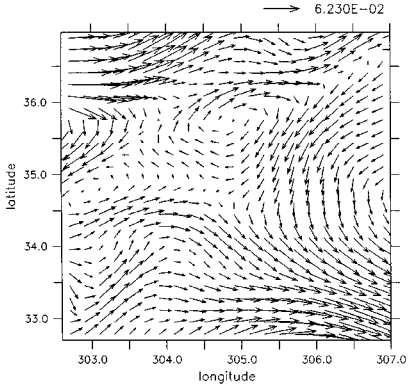
6.230E-02
latitude
longitude
36.0
35.0
34.0
33.0
303.0
304.0
305.0
306.0
307.0

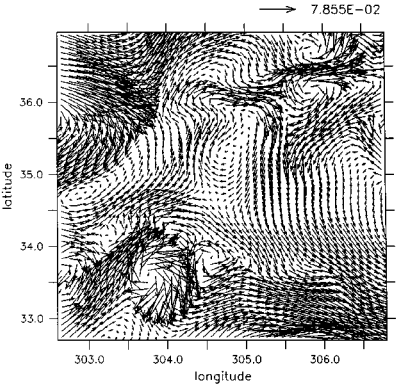
7.855E-02
latitude
longitude
36.0
35.0
34.0
33.0
303.0
304.0
305.0
306.0

we are forcing the higher resolution runs with lower resolution boundary conditions. Over a period of time, the solution in the interior of the model domain gradually begins to differ from the exterior forcing field, particularly when higher resolution is used, and this forces us to limit the length of our simulations (to about 4 months in this case). This is a limitation of this kind of regional modeling. When the model is used to selectively refine a region within a coarser large-scale model (an issue which is further discussed below), longer simulations can be achieved by "two-way" nesting the limited area model within the outer model that provides the boundary conditions. Then the solution of the outer model is modified to match the solution in the limited-area model, presumed to be more accurate because of the higher resolution used. This would keep the embedded model and its boundary conditions in synchrony and prevent problems arising from discrepancy in the resolution, but it would further propagate the solution error arising from the orthogonal boundary condition formulation described below. Figure 7 shows the time evolution of the temperature field from the 0.1° resolution model in the $10^\circ \times 10^\circ$ region of the Atlantic. The fine scale flow can be seen to develop from the smooth initial condition over a period of a few weeks and then to deteriorate in the last two weeks of the simulation as the interior solution begins to diverge from the flow field that provides the boundary conditions.

While the nonhydrostatic model simulations performed here overcome the problem of ill-posedness in open domains, they still suffer from the limitation that the boundary conditions are prescribed along characteristics only normal to the boundary. When we compare the solutions in the interior $5^\circ \times 5^\circ$ subregion of the domain obtained (a) by modeling the subregion separately at 0.2° resolution with 0.2° boundary conditions (Fig. 8, top left) and (b) by extracting the subregion from the larger domain modeled at 0.2° resolution (Fig. 8, lower left), we find that the former is not identical to the latter, as one would desire. We ascribe the differences, which are more pronounced in the more variable and faster moving upper layers of the ocean than in the interior, to the characteristics-based formulation of the boundary conditions that only propagates information normal to the boundary and assumes the nonorthogonal component to be negligible. This assumption of orthogonality does not hold very well in all cases and the error introduced as a result is not restricted just to the boundary, but propagates into the interior as well.

In this study, we have shown how we may model a region of the ocean given boundary conditions, which are assumed to be correct. In reality, such boundary conditions may come from limited data, and our intention would be to describe the interior flow by making the most of them. A slightly different issue is that of selectively refining a region of interest in one's model domain. A general difficulty in this approach is exhibited by comparing the solutions in the $5^\circ \times 5^\circ$ interior subregion (a) modeled at 0.1° with 0.2° resolution boundary conditions applied at the boundary of the interior subregion (Fig. 8, top right) and (b) extracted from the larger $10^\circ \times 10^\circ$ region modeled entirely at 0.1° resolution (Fig. 8, lower right). While both right-hand views seem to be plausible fine-scale representations of either of the left-hand views, there is considerable difference between them. The difference is not so much due to the orthogonality limitations of the boundary conditions described above, but more because 0.2° and 0.1° resolutions in the $10^\circ \times 10^\circ$ region produce different solutions on the boundary of the $5^\circ \times 5^\circ$ subregion. Hence, one ought to exercise caution when using coarse resolution initial and boundary conditions to model a region at higher resolution. The solution can only be as good as the boundary and initial conditions, and the coarse resolution ought to adequately resolve the flow until such time that one decides to selectively refine a region of it. Refinement is useful for tracking the development of a

feature of interest for as long as the feature resides in the interior of the refinement required to resolve it.

5. CONCLUSIONS

Using a nonhydrostatic set of equations, we are able to model a region of the open ocean for which initial and boundary conditions are available. The ability of the well-posed nonhydrostatic model to handle open boundaries without resorting to viscosity or any special boundary conditions is in contrast with the difficulties associated with using the hydrostatic model in the same situation. We can model the region at higher resolution than the initial and boundary data. This enables us to capture the frontal and eddy structure that is important to many ocean processes but is missed at the coarser resolution that is globally affordable or at which the data may be available. In certain appropriate situations, the model may be used to selectively refine a region of the global domain modeled at coarser resolution.

ACKNOWLEDGMENTS

We are grateful to Dr. Semtner for making the flow fields from the (1/4)-degree global circulation experiment available to us and to Dr. G. L. Browning and anonymous reviewers for some very helpful suggestions.

REFERENCES

1. R. Bleck, R. Onken, and J. D. Woods, A two-dimensional model of mesoscale frontogenesis in the ocean, *Quart. J. R. Meteorol. Soc.* **114**, 347 (1988).
2. G. L. Browning, W. R. Holland, H-O. Kreiss, and S. J. Worley, An accurate hyperbolic system for approximately hydrostatic and incompressible oceanographic flows, *Dyn. Atmos. Oceans* **14**, 303 (1990).
3. D. Chen and L. M. Rothstein, A hybrid vertial mixing scheme and its application to tropical ocean models, *J. Phys. Oceanogr.* **24**, 2156 (1994).
4. A. D. Fox and S. J. Maskell, Two-way interactive nesting of primitive equation ocean models with topography, *J. Phys. Oceanogr.* **23**, 2977 (1995).
5. S. Hellerman and M. Rosenstein, Normal monthly wind stress over the world ocean with error estimates, *J. Phys. Oceanogr.* **13**, 1093 (1983).
6. B. P. Leonard, A stable and accurate convective modeling procedure based on quadratic upstream interpolation, *Comput. Methods Appl. Mech. Eng.* **19**, 59 (1979).
7. A. Mahadevan and D. Archer, Estimating new production in the subtropical oceans: A modeling study, in preparation.
8. A. Mahadevan, J. Oliger, and R. Street, A non-hydrostatic mesoscale ocean model 2: Numerical implementation, *J. Phys. Oceanogr.* **26**(9), 1181 (1996).
9. A. Mahadevan, J. Oliger, and R. Street, A non-hydrostatic mesoscale ocean model 1: Well-posedness and scaling, *J. Phys. Oceanogr.* **26**(9), 1168 (1996).
10. A. Majda, *Compressible Fluid Flow and Systems of Conservation Laws in Several Space Variables, Applied Mathematical Sciences*, Vol. 53, Springer-Verlag, New York/Berlin, 1984.
11. J. Marshall, C. Hill, L. Perelman, and A. Adcrof, Hydorstatic, quasi-hydrostatic, and non-hydrostatic ocean modeling, *J. Geophys. Res.* **102**(C3), 5733 (1997).
12. K. Miyakoda and A. Rosati, One-way nested grid models: The interface conditions and the numerical accuracy, *Mon. Weather Rev.* **105**, 1092 (1977).
13. P. A. Newberger and J. S. Allen, On the use of the Boussinesq equations, the reduced system, and the primitive equations for the computation of geophysical flows, *Dyn. Atmos. Oceans* **25**, 1 (1996).

14. J. Oliger and A. Sundstrom, Theoretical and practical aspects of some initial boundary value problems in fluid dynamics, *SIAM J. Appl. Math.* **35**(3), 419 (1978).
15. A. J. Semtner Jr. and R. M. Chervin, Ocean general circulation from a global eddy-resolving model, *J. Geophys. Res.* **97**(c4), 5493 (1992).
16. M. A. Spall, Regional primitive equation modeling and analysis of the polymode data set, *Dyn. Atmos. Oceans* **14**, 125 (1989).
17. M. A. Spall and W. R. Holland, A nested primitive equation model for oceanic applications, *J. Phys. Oceanogr.* **21**, 205 (1991).
18. M. A. Spall and A. A. Robinson, A new open ocean, hybrid coordinate primitive equation model, *Math. Comput. Simul.* **31**, 241 (1989).
19. J. Woods, Mesoscale upwelling and primary production, in *Toward a Theory on Biological–Physical Interactions in the World Ocean* edited by B. J. Rothschild (Kluwer Academic, Dordrecht, 1988), p. 7.
20. D.-L. Zhang, H. Chang, N. L. Seaman, T. T. Warner, and J. M. Fritsch, A two-way interactive nesting procedure with variable terrain resolution, *Mon. Weather Rev.* **114**, 1330 (1986).